

**Observation of  $K^*(892)^0 \bar{K}^*(892)^0$  in  $\chi_{cJ}$  decays**

M. Ablikim,<sup>1</sup> J. Z. Bai,<sup>1</sup> Y. Ban,<sup>10</sup> J. G. Bian,<sup>1</sup> X. Cai,<sup>1</sup> J. F. Chang,<sup>1</sup> H. F. Chen,<sup>16</sup> H. S. Chen,<sup>1</sup> H. X. Chen,<sup>1</sup> J. C. Chen,<sup>1</sup> Jin Chen,<sup>1</sup> Jun Chen,<sup>6</sup> M. L. Chen,<sup>1</sup> Y. B. Chen,<sup>1</sup> S. P. Chi,<sup>2</sup> Y. P. Chu,<sup>1</sup> X. Z. Cui,<sup>1</sup> H. L. Dai,<sup>1</sup> Y. S. Dai,<sup>18</sup> Z. Y. Deng,<sup>1</sup> L. Y. Dong,<sup>1</sup> S. X. Du,<sup>1</sup> Z. Z. Du,<sup>1</sup> J. Fang,<sup>1</sup> S. S. Fang,<sup>2</sup> C. D. Fu,<sup>1</sup> H. Y. Fu,<sup>1</sup> C. S. Gao,<sup>1</sup> Y. N. Gao,<sup>14</sup> M. Y. Gong,<sup>1</sup> W. X. Gong,<sup>1</sup> S. D. Gu,<sup>1</sup> Y. N. Guo,<sup>1</sup> Y. Q. Guo,<sup>1</sup> Z. J. Guo,<sup>15</sup> F. A. Harris,<sup>15</sup> K. L. He,<sup>1</sup> M. He,<sup>1</sup> X. He,<sup>1</sup> Y. K. Heng,<sup>1</sup> H. M. Hu,<sup>1</sup> T. Hu,<sup>1</sup> G. S. Huang,<sup>1,\*</sup> L. Huang,<sup>6</sup> X. P. Huang,<sup>1</sup> X. B. Ji,<sup>1</sup> Q. Y. Jia,<sup>10</sup> C. H. Jiang,<sup>1</sup> X. S. Jiang,<sup>1</sup> D. P. Jin,<sup>1</sup> S. Jin,<sup>1</sup> Y. Jin,<sup>1</sup> Y. F. Lai,<sup>1</sup> F. Li,<sup>1</sup> G. Li,<sup>1</sup> H. H. Li,<sup>1</sup> J. Li,<sup>1</sup> J. C. Li,<sup>1</sup> Q. J. Li,<sup>1</sup> R. B. Li,<sup>1</sup> R. Y. Li,<sup>1</sup> S. M. Li,<sup>1</sup> W. G. Li,<sup>1</sup> X. L. Li,<sup>7</sup> X. Q. Li,<sup>9</sup> X. S. Li,<sup>14</sup> Y. F. Liang,<sup>13</sup> H. B. Liao,<sup>5</sup> C. X. Liu,<sup>1</sup> F. Liu,<sup>5</sup> Fang Liu,<sup>13</sup> H. M. Liu,<sup>1</sup> J. B. Liu,<sup>1</sup> J. P. Liu,<sup>17</sup> R. G. Liu,<sup>1</sup> Z. A. Liu,<sup>1</sup> Z. X. Liu,<sup>1</sup> F. Lu,<sup>1</sup> G. R. Lu,<sup>4</sup> J. G. Lu,<sup>1</sup> C. L. Luo,<sup>8</sup> X. L. Luo,<sup>1</sup> F. C. Ma,<sup>7</sup> J. M. Ma,<sup>1</sup> L. L. Ma,<sup>11</sup> Q. M. Ma,<sup>1</sup> X. Y. Ma,<sup>1</sup> Z. P. Mao,<sup>1</sup> X. H. Mo,<sup>1</sup> J. Nie,<sup>1</sup> Z. D. Nie,<sup>1</sup> S. L. Olsen,<sup>15</sup> H. P. Peng,<sup>16</sup> N. D. Qi,<sup>1</sup> C. D. Qian,<sup>12</sup> H. Qin,<sup>8</sup> J. F. Qiu,<sup>1</sup> Z. Y. Ren,<sup>1</sup> G. Rong,<sup>1</sup> L. Y. Shan,<sup>1</sup> L. Shang,<sup>1</sup> D. L. Shen,<sup>1</sup> X. Y. Shen,<sup>1</sup> H. Y. Sheng,<sup>1</sup> F. Shi,<sup>1</sup> X. Shi,<sup>10</sup> H. S. Sun,<sup>1</sup> S. S. Sun,<sup>16</sup> Y. Z. Sun,<sup>1</sup> Z. J. Sun,<sup>1</sup> X. Tang,<sup>1</sup> N. Tao,<sup>16</sup> Y. R. Tian,<sup>14</sup> G. L. Tong,<sup>1</sup> G. S. Varner,<sup>15</sup> D. Y. Wang,<sup>1</sup> J. Z. Wang,<sup>1</sup> K. Wang,<sup>16</sup> L. Wang,<sup>1</sup> L. S. Wang,<sup>1</sup> M. Wang,<sup>1</sup> P. Wang,<sup>1</sup> P. L. Wang,<sup>1</sup> S. Z. Wang,<sup>1</sup> W. F. Wang,<sup>1</sup> Y. F. Wang,<sup>1</sup> Zhe Wang,<sup>1</sup> Z. Wang,<sup>1</sup> Zheng Wang,<sup>1</sup> Z. Y. Wang,<sup>1</sup> C. L. Wei,<sup>1</sup> D. H. Wei,<sup>3</sup> N. Wu,<sup>1</sup> Y. M. Wu,<sup>1</sup> X. M. Xia,<sup>1</sup> X. X. Xie,<sup>1</sup> B. Xin,<sup>7</sup> G. F. Xu,<sup>1</sup> H. Xu,<sup>1</sup> Y. Xu,<sup>1</sup> S. T. Xue,<sup>1</sup> M. L. Yan,<sup>16</sup> F. Yang,<sup>9</sup> H. X. Yang,<sup>1</sup> J. Yang,<sup>16</sup> S. D. Yang,<sup>1</sup> Y. X. Yang,<sup>3</sup> M. Ye,<sup>1</sup> M. H. Ye,<sup>2</sup> Y. X. Ye,<sup>16</sup> L. H. Yi,<sup>6</sup> Z. Y. Yi,<sup>1</sup> C. S. Yu,<sup>1</sup> G. W. Yu,<sup>1</sup> C. Z. Yuan,<sup>1</sup> J. M. Yuan,<sup>1</sup> Y. Yuan,<sup>1</sup> Q. Yue,<sup>1</sup> S. L. Zang,<sup>1</sup> Yu. Zeng,<sup>1</sup> Y. Zeng,<sup>6</sup> B. X. Zhang,<sup>1</sup> B. Y. Zhang,<sup>1</sup> C. C. Zhang,<sup>1</sup> D. H. Zhang,<sup>1</sup> H. Y. Zhang,<sup>1</sup> J. Zhang,<sup>1</sup> J. Y. Zhang,<sup>1</sup> J. W. Zhang,<sup>1</sup> L. S. Zhang,<sup>1</sup> Q. J. Zhang,<sup>1</sup> S. Q. Zhang,<sup>1</sup> X. M. Zhang,<sup>1</sup> X. Y. Zhang,<sup>11</sup> Y. J. Zhang,<sup>10</sup> Y. Y. Zhang,<sup>1</sup> Yiyun Zhang,<sup>13</sup> Z. P. Zhang,<sup>16</sup> Z. Q. Zhang,<sup>4</sup> D. X. Zhao,<sup>1</sup> J. B. Zhao,<sup>1</sup> J. W. Zhao,<sup>1</sup> M. G. Zhao,<sup>9</sup> P. P. Zhao,<sup>1</sup> W. R. Zhao,<sup>1</sup> X. J. Zhao,<sup>1</sup> Y. B. Zhao,<sup>1</sup> Z. G. Zhao,<sup>1,†</sup> H. Q. Zheng,<sup>10</sup> J. P. Zheng,<sup>1</sup> L. S. Zheng,<sup>1</sup> Z. P. Zheng,<sup>1</sup> X. C. Zhong,<sup>1</sup> B. Q. Zhou,<sup>1</sup> G. M. Zhou,<sup>1</sup> L. Zhou,<sup>1</sup> N. F. Zhou,<sup>1</sup> K. J. Zhu,<sup>1</sup> Q. M. Zhu,<sup>1</sup> Y. C. Zhu,<sup>1</sup> Y. S. Zhu,<sup>1</sup> Yingchun Zhu,<sup>1</sup> Z. A. Zhu,<sup>1</sup> B. A. Zhuang,<sup>1</sup> and B. S. Zou<sup>1</sup>

(BES Collaboration)

<sup>1</sup>*Institute of High Energy Physics, Beijing 100039, People's Republic of China*<sup>2</sup>*China Center of Advanced Science and Technology, Beijing 100080, People's Republic of China*<sup>3</sup>*Guangxi Normal University, Guilin 541004, People's Republic of China*<sup>4</sup>*Henan Normal University, Xinxiang 453002, People's Republic of China*<sup>5</sup>*Huazhong Normal University, Wuhan 430079, People's Republic of China*<sup>6</sup>*Hunan University, Changsha 410082, People's Republic of China*<sup>7</sup>*Liaoning University, Shenyang 110036, People's Republic of China*<sup>8</sup>*Nanjing Normal University, Nanjing 210097, People's Republic of China*<sup>9</sup>*Nankai University, Tianjin 300071, People's Republic of China*<sup>10</sup>*Peking University, Beijing 100871, People's Republic of China*<sup>11</sup>*Shandong University, Jinan 250100, People's Republic of China*<sup>12</sup>*Shanghai Jiaotong University, Shanghai 200030, People's Republic of China*<sup>13</sup>*Sichuan University, Chengdu 610064, People's Republic of China*<sup>14</sup>*Tsinghua University, Beijing 100084, People's Republic of China*<sup>15</sup>*University of Hawaii, Honolulu, Hawaii 96822, USA*<sup>16</sup>*University of Science and Technology of China, Hefei 230026, People's Republic of China*<sup>17</sup>*Wuhan University, Wuhan 430072, People's Republic of China*<sup>18</sup>*Zhejiang University, Hangzhou 310028, People's Republic of China*

(Received 5 August 2004; published 9 November 2004)

$K^*(892)^0 \bar{K}^*(892)^0$  signals from  $\chi_{cJ}(J = 0, 1, 2)$  decays are observed for the first time using a data sample of 14 million  $\psi(2S)$  events accumulated in the BES II detector. The branching fractions  $\mathcal{B}[\chi_{cJ} \rightarrow K^*(892)^0 \bar{K}^*(892)^0]$  ( $J = 0, 1, 2$ ) are determined to be  $(1.78 \pm 0.34 \pm 0.34) \times 10^{-3}$ ,  $(1.67 \pm 0.32 \pm 0.31) \times 10^{-3}$ , and  $(4.86 \pm 0.56 \pm 0.88) \times 10^{-3}$  for the  $\chi_{c0}$ ,  $\chi_{c1}$ , and  $\chi_{c2}$  decays, respectively, where the first errors are statistical and the second are systematic. The significances of these signals are about  $4.7\sigma$ ,  $4.5\sigma$ , and  $7.6\sigma$ , respectively.

\*Current address: Purdue University, West Lafayette, Indiana 47907, USA.

†Visiting professor to University of Michigan, Ann Arbor, Michigan 48109, USA.

## I. INTRODUCTION

Exclusive quarkonium decays constitute an important laboratory for investigating perturbative quantum chromodynamics. In the case of  $P$ -wave charmonium  $\chi_{cJ}$  decays to a pair of pseudoscalars, one finds that the lowest Fock state, the color-singlet contribution, alone is not sufficient to accommodate the data. Indeed, the color-octet contribution from the next higher Fock state contributes at the same level as the color-singlet one. Its inclusion yields good agreement with experimental data [1,2]. The calculation of the partial width of  $\chi_{cJ} \rightarrow p\bar{p}$ , taking into account the color-octet mechanism [3], also gives results in reasonable agreement with measurements [4,5]. However, a recent measurement of  $\chi_{cJ} \rightarrow \Lambda\bar{\Lambda}$  [6] agrees poorly with the prediction, including the color-octet contribution, for this process.

Compared to  $J/\psi$  decays, relatively little is known concerning  $PC = ++$   $\chi_{cJ}$  decays. Only a few two-body decays have been measured. For these theoretical predictions exist, but there are no predictions for the majority of hadronic decay modes. Current theoretical analyses of the  $\chi_{cJ}$  decays provide only a rough treatment of the color-octet wave function. A reanalysis of the decays into pseudoscalar-pseudoscalar and baryon antibaryon channels, as well as the extension to vector-vector, is required [7]. At present only one  $\chi_{cJ}$  to vector-vector ( $\chi_{cJ} \rightarrow \phi\phi$ ) branching fraction has been measured experimentally. A consistent set of predictions for the branching fractions, as well as more precise experimental measurements, for a number of the two-body decays will lead to a better understanding of the color-octet mechanism and the nature of  $3P_J c\bar{c}$  bound states.

Further, the decays of  $\chi_{cJ}$ , in particular  $\chi_{c0}$  and  $\chi_{c2}$ , provide a direct window on glueball dynamics in the  $0^{++}$  and  $2^{++}$  channels, as the hadronic decays may proceed via  $c\bar{c} \rightarrow gg \rightarrow q\bar{q}q\bar{q}$  [8].

Recently, the branching fraction for  $\chi_{c0} \rightarrow f_0(980)f_0(980)$  was reported by BES [9]. In this paper, we report on the analysis of  $\pi^+\pi^-K^+K^-$  final states from  $\chi_{cJ}(J=0,1,2)$  decays using 14 million  $\psi(2S)$  events accumulated at the upgraded BES detector (BES II). Signals of  $\chi_{c0}$ ,  $\chi_{c1}$ , and  $\chi_{c2}$  decays to  $K^*(892)^0\bar{K}^*(892)^0$  in  $\psi(2S)$  radiative decays are observed for the first time.

## II. BES DETECTOR

BES II is a large solid-angle magnetic spectrometer that is described in detail in Ref. [10]. Charged particle momenta are determined with a resolution of  $\sigma_p/p = 1.78\%\sqrt{1+p^2}$  ( $p$  in GeV/ $c$ ) in a 40-layer cylindrical drift chamber. Particle identification is accomplished by specific ionization ( $dE/dx$ ) measurements in the drift

chamber and time-of-flight (TOF) measurements in a barrel-like array of 48 scintillation counters. The  $dE/dx$  resolution is  $\sigma_{dE/dx} = 8.0\%$ ; the TOF resolution is  $\sigma_{\text{TOF}} = 180$  ps for Bhabha events. Outside of the time-of-flight counters is a 12-radiation-length barrel shower counter (BSC) comprised of gas tubes interleaved with lead sheets. The BSC measures the energies of photons with a resolution of  $\sigma_E/E \simeq 21\%/\sqrt{E}$  ( $E$  in GeV). Outside the solenoidal coil, which provides a 0.4 T magnetic field over the tracking volume, is an iron flux return that is instrumented with three double layers of counters that are used to identify muons.

In this analysis, a GEANT3 based Monte Carlo simulation package (SIMBES) with detailed consideration of detector performance (such as dead electronic channels) is used. The consistency between data and Monte Carlo has been checked in many high purity physics channels, and the agreement is quite reasonable.

## III. EVENT SELECTION

The selection criteria described below are similar to those used in a previous BES analysis [11].

### A. Photon identification

A neutral cluster is considered to be a photon candidate when the angle between the nearest charged track and the cluster is greater than  $15^\circ$ , the first hit is in the beginning six radiation lengths, and the difference between the angle of the cluster development direction in the BSC and the photon emission direction is less than  $30^\circ$ . The photon candidate with the largest energy deposit in the BSC is treated as the photon radiated from  $\psi(2S)$  and used in a four-constraint kinematic fit to the hypothesis  $\psi(2S) \rightarrow \gamma\pi^+\pi^-K^+K^-$ .

### B. Charged particle identification

Each charged track, reconstructed using the MDC information, is required to be well fit to a three-dimensional helix, be in the polar angle region  $|\cos\theta_{\text{MDC}}| < 0.80$ , and have the point of closest approach of the track to the beam axis be within 2 cm of the beam axis and within 20 cm from the center of the interaction region along the beam line. For each track, the TOF and  $dE/dx$  measurements are used to calculate  $\chi^2$  values and the corresponding confidence levels for the hypotheses that the particle is a pion, kaon, or proton ( $\text{Prob}_\pi$ ,  $\text{Prob}_K$ ,  $\text{Prob}_p$ ).

### C. Event selection criteria

Candidate events are required to satisfy the following selection criteria:

- (1) The number of charged tracks is required to be four with net charge zero.
- (2) The sum of the momenta of the two lowest momentum tracks is required to be greater than  $650 \text{ MeV}/c$ ; this removes contamination from  $\psi(2S) \rightarrow \pi^+ \pi^- J/\psi$  events and some of the  $K^* K \pi$  background.
- (3) The  $\chi^2$  probability for the four-constraint kinematic fit to the decay hypothesis  $\psi(2S) \rightarrow \gamma \pi^+ \pi^- K^+ K^-$  is required to be greater than 0.01.

A combined probability determined from the four-constraint kinematic fit and particle identification information is used to separate  $\gamma \pi^+ \pi^- \pi^+ \pi^-$ ,  $\gamma K^+ K^- K^+ K^-$ , and the different possible particle assignments for the  $\gamma \pi^+ \pi^- K^+ K^-$  final states. This combined probability,  $\text{Prob}_{\text{all}}$ , is defined as

$$\text{Prob}_{\text{all}} = \text{Prob}(\chi_{\text{all}}^2, \text{ndf}_{\text{all}}),$$

where  $\chi_{\text{all}}^2$  is the sum of the  $\chi^2$  values from the four-constraint kinematic fit and those from each of the four particle identification assignments, and  $\text{ndf}_{\text{all}}$  is the corresponding total number of degrees of freedom. For an event to be selected,  $\text{Prob}_{\text{all}}$  of the  $\gamma \pi^+ \pi^- K^+ K^-$  must be larger than those of the other possibilities. In addition, the particle identification probability of each charged track  $\text{Prob}_{\text{ID}}$  must be  $>0.01$ .

The invariant mass distribution for the  $\pi^+ \pi^- K^+ K^-$  events that survive all the selection requirements is shown

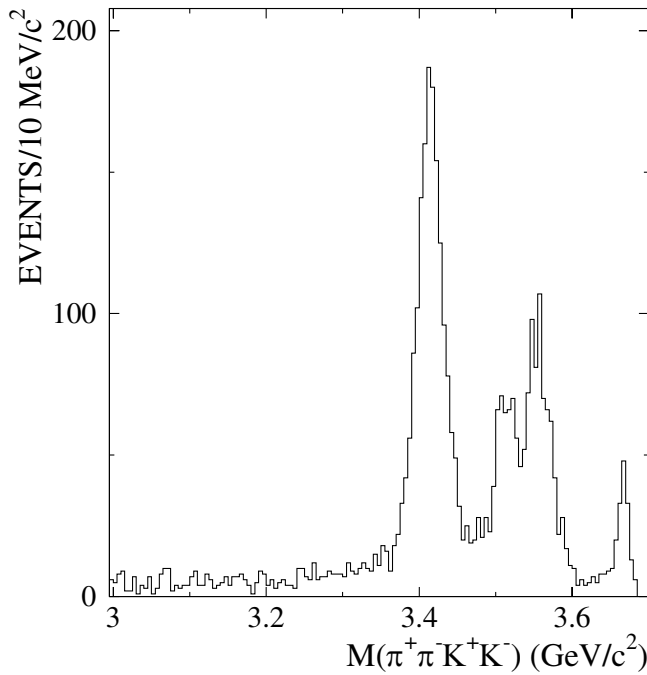


FIG. 1. The  $\pi^+ \pi^- K^+ K^-$  invariant mass spectrum. There are three clear  $\chi_{cJ}$  peaks. The highest mass peak corresponds to charged track final states that are kinematically fit with an unassociated, low energy photon.

in Fig. 1. There are clear peaks corresponding to the  $\chi_{cJ}$  states. The highest mass peak corresponds to charged track final states that are kinematically fit with an unassociated, low energy photon.

#### IV. ANALYSIS RESULTS

The scatter plots of  $K^- \pi^+$  versus  $K^+ \pi^-$  invariant masses for events with a  $\pi^+ \pi^- K^+ K^-$  mass within (3.30, 3.48), (3.48, 3.53), and (3.53, 3.65)  $\text{GeV}/c^2$  are shown in Fig. 2. Clear  $K^*(892)^0 \bar{K}^*(892)^0$  signals can be seen in all  $\chi_{cJ}$  decays, as well as some hints of  $K_2^*(1430)^0 \bar{K}_2^*(1430)^0$  [or  $K_0^*(1430)^0 \bar{K}_0^*(1430)^0$ ] and  $K_1(1270) \bar{K} + \text{c.c.}$  [or  $K_1(1400) \bar{K} + \text{c.c.}$ ] signals. In this paper, we study  $K^*(892)^0 \bar{K}^*(892)^0$  production in  $\chi_{c0,1,2}$  decays.

##### A. $K^*(892)^0 \bar{K}^*(892)^0$ signal

For events in the  $\chi_{cJ}$  mass region between 3.30 and 3.65  $\text{GeV}/c^2$ , if the mass of one or both  $K\pi$  pairs is in the  $K^*(892)$  mass region between 0.836 and 0.956  $\text{GeV}/c^2$ , the mass of the other  $K\pi$  pair is plotted, as shown in Fig. 3; there is a strong  $K^*(892)$  signal. The distribution is fitted with a background polynomial plus a  $P$ -wave relativistic Breit-Wigner function, with a width

$$\Gamma = \Gamma_0 \frac{m_0}{m} \frac{1 + r^2 p_0^2}{1 + r^2 p^2} \left[ \frac{p}{p_0} \right]^3,$$

where  $m$  is the mass of the  $K\pi$  system,  $p$  is the momentum of kaon in the  $K\pi$  system,  $\Gamma_0$  is the width of the resonance,  $m_0$  is the mass of the resonance,  $p_0$  is  $p$  evaluated at the resonance mass,  $r$  is the interaction radius, and  $(1 + r^2 p_0^2)/(1 + r^2 p^2)$  represents the contribution of the barrier factor. The fit of Fig. 3 gives an  $r$  value of  $(3.4 \pm 2.6) (\text{GeV}/c)^{-1}$  with a large error due to the low statistics. Therefore, in later analysis (mainly in the efficiency calculation), we use the value  $(3.4 \pm 0.6 \pm 0.3) (\text{GeV}/c)^{-1}$  measured by a  $K^- \pi^+$  scattering experiment [12] for  $r$ .

In this paper, the number of  $K^*(892)^0 \bar{K}^*(892)^0$  events and the corresponding background are estimated from the scatter plot of  $K^- \pi^+$  versus  $K^+ \pi^-$  invariant masses, as shown in Fig. 4. The signal region is shown as a square box (solid line) at (0.896, 0.896)  $\text{GeV}/c^2$  with the width of 60  $\text{MeV}/c^2$ . From a Monte Carlo study, a large background comes from  $\psi(2S) \rightarrow \gamma \chi_{cJ} \rightarrow \gamma K_1(1270) \bar{K} + \text{c.c.}$  [or  $K_1(1400) \bar{K} + \text{c.c.}$ ] which decays to  $\gamma \pi^+ \pi^- K^+ K^-$  final states via  $K_1 \rightarrow K^*(892) \pi$  intermediate decay. This background shows up as the horizontal and vertical bands at  $m[K^*(892)]$  in the  $m(K^- \pi^+)$  versus  $m(K^+ \pi^-)$  scatter plots of Fig. 2. The background is estimated from the sideband boxes, which are taken 60  $\text{MeV}/c^2$  away from the signal box and shown as four dashed-line and four dotted-line boxes in Fig. 4. The horizontal and vertical

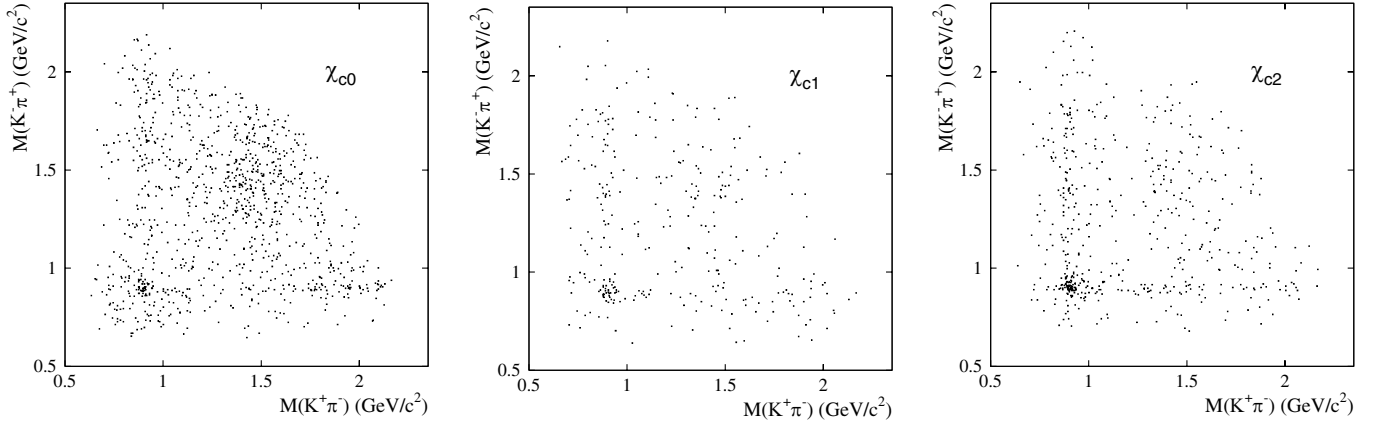


FIG. 2. Scatter plots of  $K^- \pi^+$  versus  $K^+ \pi^-$  invariant masses for selected  $\gamma \pi^+ \pi^- K^+ K^-$  events with  $\pi^+ \pi^- K^+ K^-$  mass in  $\chi_{c0}$ ,  $\chi_{c1}$ , and  $\chi_{c2}$  mass regions, respectively. Clear  $K^*(892)^0 \bar{K}^*(892)^0$  signals can be seen in all  $\chi_{cJ}$  decays, as well as some hints of  $K_2^*(1430)^0 \bar{K}_2^*(1430)^0$  [or  $K_0^*(1430)^0 \bar{K}_0^*(1430)^0$ ] and  $K_1(1270) \bar{K} + \text{c.c.}$  [or  $K_1(1400) \bar{K} + \text{c.c.}$ ] signals.

sideband boxes (dashed line) allow the determination of the backgrounds from the horizontal and vertical bands; the diagonal boxes (dotted lines) allow the estimation of the smaller uniform background contribution. The background in the signal region is one-half the sum of the events in the horizontal and vertical boxes minus one-quarter of the sum of the events in the diagonal boxes.

Figure 5 shows the mass distribution of the  $K^*(892)^0 \bar{K}^*(892)^0$  candidate events and the corresponding background. In the signal box for the mass region from 3.20 to 3.70  $\text{GeV}/c^2$ , there are 154 total events and 38 background events, estimated from the eight boxes as described above.

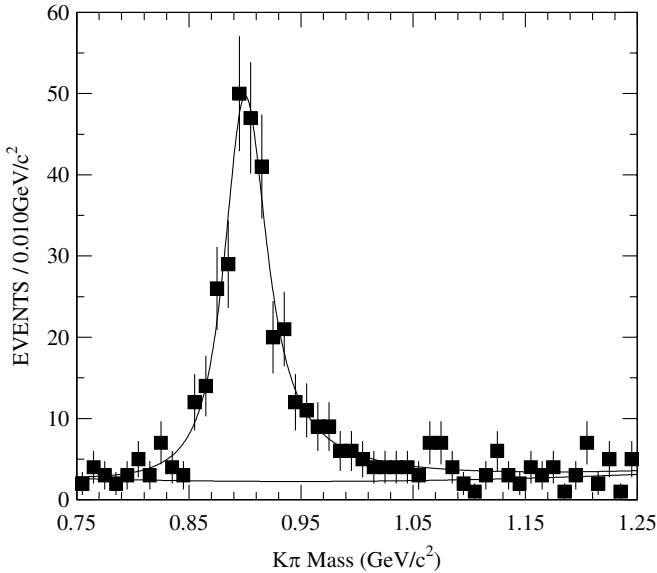


FIG. 3.  $K\pi$  invariant mass spectrum for events in the  $\chi_{cJ}$  mass region when the other (one or both)  $K\pi$  pair lies in the  $K^*(892)$  mass region between 0.836 and 0.956  $\text{GeV}/c^2$ . The curves are the Breit-Wigner function and background polynomial described in the text.

### B. Fit of the mass spectrum

After background subtraction, the  $K^*(892)^0 \bar{K}^*(892)^0$  mass spectrum between 3.20 and 3.70  $\text{GeV}/c^2$  is fitted using a  $\chi^2$  method with three Breit-Wigner functions folded with Gaussian resolutions, where the mass resolutions are fixed at their Monte Carlo predicted values [(12.2  $\pm$  0.4), (12.3  $\pm$  0.3), and (12.2  $\pm$  0.3)  $\text{MeV}/c^2$  for  $\chi_{c0}$ ,  $\chi_{c1}$ , and  $\chi_{c2}$ , respectively] and the widths of the three  $\chi_{cJ}$  states are set at their world average values [4]. A  $\chi^2$  probability of 69% is obtained, indicating a reliable fit. The number of events determined from the fit are  $30.1 \pm 5.7$ ,  $28.4 \pm 5.5$ , and  $57.5 \pm 6.4$  for  $\chi_{c0}$ ,  $\chi_{c1}$ , and  $\chi_{c2}$ ,

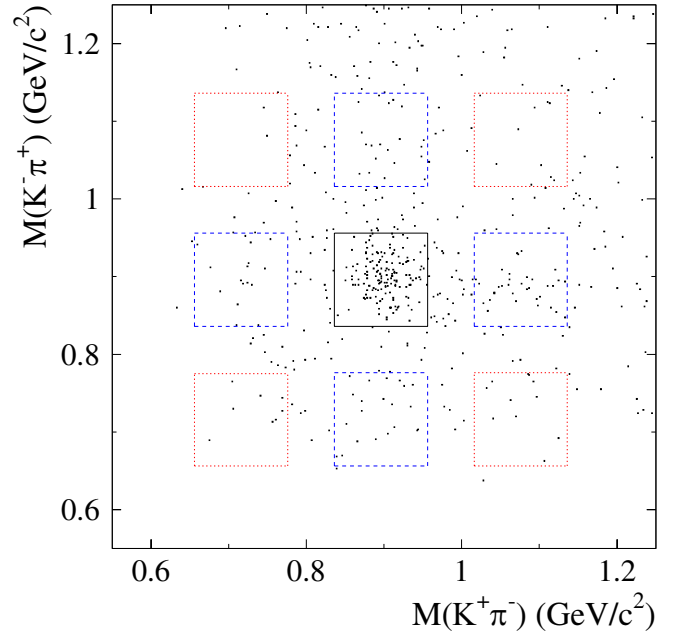


FIG. 4 (color online). Definition of signal and sideband regions. The background calculation using sidebands is described in the text.

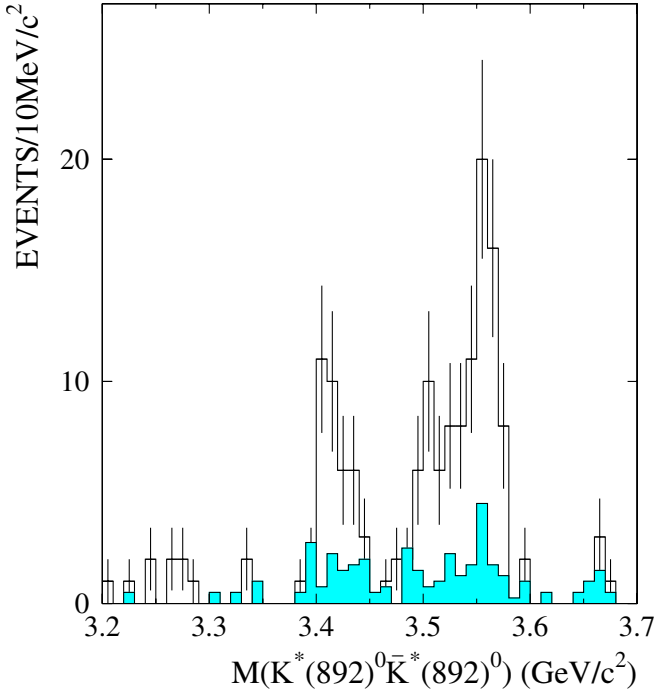


FIG. 5 (color online). The  $K^*(892)^0\bar{K}^*(892)^0$  invariant mass spectrum for events in the signal region of Fig. 4. The shaded histogram indicates the distribution of the background estimated from events in the sideband regions of Fig. 4 as described in the text.

respectively. The statistical significances of the three states are  $4.7\sigma$ ,  $4.5\sigma$ , and  $7.6\sigma$ , calculated from  $\sqrt{\Delta\chi^2}$ , where  $\Delta\chi^2$  is the difference between the  $\chi^2$  values of the fits determined with and without the signal function. Figure 6 shows the fit result, and the fitted masses are  $3415.9 \pm 3.1$ ,  $3508.4 \pm 3.6$ , and  $3553.5 \pm 1.8$  MeV/ $c^2$  for  $\chi_{c0}$ ,  $\chi_{c1}$ , and  $\chi_{c2}$ , respectively, in agreement with the world average values [4].

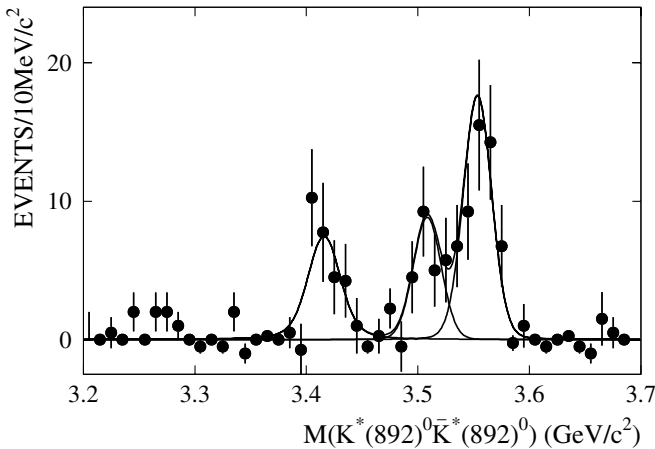


FIG. 6. The  $K^*(892)^0\bar{K}^*(892)^0$  invariant mass spectrum fitted with three resolution smeared Breit-Wigner functions as described in the text.

A Monte Carlo simulation is used to determine the detection efficiency. The angular distribution of the photon emitted in  $\psi(2S) \rightarrow \gamma\chi_{cJ}$  is taken into account [13]. The  $K^*(892)$  is generated as a  $P$ -wave relativistic Breit-Wigner with  $r$  as  $3.4$  (GeV/ $c$ ) $^{-1}$  [12]. For each case, 50 000 Monte Carlo events are simulated, and the efficiencies are estimated to be  $\epsilon_{\chi_{c0}} = (3.16 \pm 0.09)\%$ ,  $\epsilon_{\chi_{c1}} = (3.26 \pm 0.09)\%$ , and  $\epsilon_{\chi_{c2}} = (2.97 \pm 0.08)\%$ , where the error is the statistical error of the Monte Carlo sample. Note that, for the efficiency estimation, the events in the eight sideband boxes are used to determine “background” which is subtracted from the events in the signal region of the scatter plot, similar to the treatment of data.

The branching fraction of  $\psi(2S) \rightarrow \gamma\chi_{cJ}$ ,  $\chi_{cJ} \rightarrow K^*(892)^0\bar{K}^*(892)^0$  is calculated using

$$\begin{aligned} \mathcal{B}[\psi(2S) \rightarrow \gamma\chi_{cJ}]\mathcal{B}[\chi_{cJ} \rightarrow K^*(892)^0\bar{K}^*(892)^0] \\ = \frac{n^{\text{obs}}/(\epsilon \cdot f^2)}{N_{\psi(2S)}}, \end{aligned}$$

where the factor  $f$  is the branching fraction of  $K^*(892)^0$  to the charged  $K\pi$  mode, which is taken as  $\frac{2}{3}$ . Using the numbers obtained above and the total number of  $\psi(2S)$  events,  $14.0(1.00 \pm 0.04) \times 10^6$  [14], we determine the product branching fractions listed in Table II.

### C. Systematic errors

The systematic errors in the branching fraction measurement associated with the efficiency are determined by comparing  $\psi(2S)$  data and Monte Carlo simulation for very clean decay channels, such as  $\psi(2S) \rightarrow \pi^+\pi^-J/\psi$ , which allows the determination of systematic errors associated with the MDC tracking, kinematic fitting, particle identification, and efficiency of the photon ID [15]. Other sources of systematic error come from the uncertainties in the number of  $\psi(2S)$  events [14], the efficiency estimation using simulated data, the background, the  $\chi_{cJ}$  and  $K^*(892)^0$  mass resolutions, the binning and fit range, etc.

#### 1. Efficiency estimation

As mentioned above, we use the measurement of Ref. [12],  $(3.4 \pm 0.6 \pm 0.3)$  (GeV/ $c$ ) $^{-1}$  for  $r$  in the  $P$ -wave relativistic Breit-Wigner parametrization in the Monte Carlo simulation. We also use  $r$  varied by one sigma to  $2.73$  and  $4.07$  (GeV/ $c$ ) $^{-1}$  to determine the change in the detection efficiency. For  $r = 2.73$  (GeV/ $c$ ) $^{-1}$ , the efficiencies of the  $\chi_{c0}$ ,  $\chi_{c1}$ , and  $\chi_{c2}$  become  $2.91\%$ ,  $3.00\%$ , and  $2.75\%$ , and for  $r = 4.07$  (GeV/ $c$ ) $^{-1}$  the corresponding efficiencies are  $3.37\%$ ,  $3.52\%$ , and  $3.17\%$ , respectively. The largest changes are about  $7.9\%$ ,  $8.0\%$ , and  $7.4\%$  for  $\chi_{c0}$ ,  $\chi_{c1}$ , and  $\chi_{c2}$ .

TABLE I. Summary of systematic errors in the branching fraction calculation of  $\mathcal{B}[\psi(2S) \rightarrow \gamma\chi_{cJ}]\mathcal{B}(\chi_{cJ} \rightarrow K^*(892)^0\bar{K}^*(892)^0)$ .

Source	$\chi_{c0}$	$\chi_{c1}$	$\chi_{c2}$
MDC tracking	8%	8%	8%
Kinematic fit	6%	6%	6%
Particle identification	5%	5%	5%
Photon ID efficiency	2%	2%	2%
$\psi(2S)$ number	4%	4%	4%
Efficiency estimation	7.9%	8.0%	7.4%
Background	7.0%	5.5%	4.5%
Mass resolutions	5%	3.5%	3.5%
Binning and fit range	3%	2%	2%
Total systematic error	17.0%	16.0%	15.4%

## 2. Background subtraction

In Sec. IVA, the backgrounds are estimated using the sidebands shown as the four dashed-line and four dotted-line boxes in Fig. 4. Moving the sideband boxes 20 MeV/ $c^2$  away from or closer to the signal region, using three instead of four dotted-line boxes (and dividing by three), or varying the background number by 1 standard deviation, the largest changes of the branching fractions for the  $\chi_{c0}$ ,  $\chi_{c1}$ , and  $\chi_{c2}$  are about 7.0%, 5.5%, and 4.5%, respectively, obtained by refitting the  $K^*(892)^0\bar{K}^*(892)^0$  mass spectrum and reestimating the efficiency.

## 3. $\chi_{cJ}$ and $K^*(892)^0$ mass resolutions

Differences between data and Monte Carlo for the mass resolutions of the  $\chi_{cJ}$  or  $K^*(892)^0$  also give uncertainties in the determination of the branching fractions. The maximum possible difference for  $\chi_{cJ}$  is about 1 MeV/ $c^2$ . Such a change results in about 4.5%, 2.5%, and 2.0% variations in the fitted number of  $\chi_{c0}$ ,  $\chi_{c1}$ , and  $\chi_{c2}$  events. If we change the  $K^*(892)^0$  window to  $[0.836 + 0.002, 0.956 - 0.002]$  GeV/ $c^2$  and  $[0.836 - 0.002, 0.956 + 0.002]$  GeV/ $c^2$ , the efficiency variations of the  $\chi_{c0}$ ,  $\chi_{c1}$ , and  $\chi_{c2}$  are 1.5%, 2.5%, and 2.4%,

respectively. By varying the width of  $\chi_{c0}$  by  $1\sigma$ , 0.8 MeV/ $c^2$ , there is almost no change in the final fit result. We use total systematic errors of 5%, 3.5%, and 3.5% for this uncertainty.

## 4. Binning and fit range

Using different binning and fit ranges for the  $K^*(892)^0\bar{K}^*(892)^0$  mass spectrum fit yields errors of about 3%, 2%, and 2% for  $\chi_{c0}$ ,  $\chi_{c1}$ , and  $\chi_{c2}$ , respectively.

The systematic errors from all sources are listed in Table I, as are the total errors of 17.0%, 16.0%, and 15.4% for  $\chi_{c0}$ ,  $\chi_{c1}$ , and  $\chi_{c2}$ , respectively, obtained by adding them in quadrature. The resulting product branching fractions including systematic errors are given in Table II. With the Particle Data Group world average values of  $\psi(2S) \rightarrow \gamma\chi_{cJ}$  [4], we get the branching fractions  $\mathcal{B}[\chi_{cJ} \rightarrow K^*(892)^0\bar{K}^*(892)^0]$ , which are also listed in Table II. The branching fractions  $\mathcal{B}[\chi_{c0} \rightarrow K^*(892)^0\bar{K}^*(892)^0]$  and  $\mathcal{B}[\chi_{c2} \rightarrow K^*(892)^0\bar{K}^*(892)^0]$  can be compared to those of  $\mathcal{B}(\chi_{c0} \rightarrow \phi\phi) = (1.0 \pm 0.6) \times 10^{-3}$  and  $\mathcal{B}(\chi_{c2} \rightarrow \phi\phi) = (2.4 \pm 0.9) \times 10^{-3}$  [4], which are the only vector-vector decays measured previously. It is noted that the  $\chi_{c2}$  branching fractions are more than twice the  $\chi_{c0}$  branching fractions for both vector-vector decays.

## V. SUMMARY

In summary,  $K^*(892)^0\bar{K}^*(892)^0$  signals from  $\chi_{cJ}$  ( $J = 0, 1, 2$ ) decays are observed for the first time using a sample of 14 million  $\psi(2S)$  events accumulated at the BES II detector. Branching fractions are determined. They will be helpful in understanding the nature of  $\chi_c$  states.

## ACKNOWLEDGMENTS

We wish to thank Frank Close for useful comments. The BES collaboration thanks the staff of BEPC for their hard efforts. This work is supported in part by the National Natural Science Foundation of China under Contracts No. 19991480, No. 10225524, and No. 10225525, the Chinese Academy of Sciences under

TABLE II. Summary of numbers used in the branching fraction calculation and branching fraction results.

Quantity	$\chi_{c0}$	$\chi_{c1}$	$\chi_{c2}$
$n^{\text{obs}}$	$30.1 \pm 5.7$	$28.4 \pm 5.5$	$57.5 \pm 6.4$
$\epsilon(\%)$	$3.16 \pm 0.09$	$3.26 \pm 0.09$	$2.97 \pm 0.08$
$N_{\psi(2S)}(10^6)$ [14]	$14.0 \pm 0.6$	$14.0 \pm 0.6$	$14.0 \pm 0.6$
$f$	$\frac{2}{3}$	$\frac{2}{3}$	$\frac{2}{3}$
$\mathcal{B}[\psi(2S) \rightarrow \gamma\chi_{cJ}]\mathcal{B}[\chi_{cJ} \rightarrow K^*(892)^0\bar{K}^*(892)^0]$ ( $10^{-4}$ )	$1.53 \pm 0.29 \pm 0.26$	$1.40 \pm 0.27 \pm 0.22$	$3.11 \pm 0.36 \pm 0.48$
$\mathcal{B}[\psi(2S) \rightarrow \gamma\chi_{cJ}]$ (%) [4]	$8.6 \pm 0.7$	$8.4 \pm 0.8$	$6.4 \pm 0.6$
$\mathcal{B}[\chi_{cJ} \rightarrow K^*(892)^0\bar{K}^*(892)^0]$ ( $10^{-3}$ )	$1.78 \pm 0.34 \pm 0.34$	$1.67 \pm 0.32 \pm 0.31$	$4.86 \pm 0.56 \pm 0.88$

Contract No. KJ 95T-03, the 100 Talents Program of CAS under Contracts No. U-11, No. U-24, and No. U-25, and the Knowledge Innovation Project of CAS under Contracts No. U-602 and No. U-34 (IHEP); by the National Natural Science Foundation of China under

Contracts No. 10175060 (USTC) and No. 10225522 (Tsinghua University); and by the Department of Energy under Contract No. DE-FG03-94ER40833 (University of Hawaii).

- 
- [1] G. T. Bodwin, E. Braaten, and G. P. Lepage, Phys. Rev. D **51**, 1125 (1995); J. Bolz, P. Koll, and G. A. Schuler, Phys. Lett. B **392**, 198 (1997); G. A. Schuler, Nucl. Phys. B, Proc. Suppl. **64**, 450 (1998).
- [2] BES Collaboration, J. Z. Bai *et al.*, Phys. Rev. Lett. **81**, 3091 (1998).
- [3] S. M. H. Wong, Eur. Phys. J. C **14**, 643 (2000).
- [4] Particle Data Group, S. Eidelman *et al.*, Phys. Lett. B **592**, 1 (2004).
- [5] BES Collaboration, J. Z. Bai *et al.*, Phys. Lett. B **591**, 42 (2004).
- [6] BES Collaboration, J. Z. Bai *et al.*, Phys. Rev. D **67**, 112001 (2003).
- [7] Quarkonium Working Group (to be published).
- [8] C. Amsler and F. Close, Phys. Rev. D **53**, 295 (1996).
- [9] BES Collaboration, J. Z. Bai *et al.*, hep-ex/0406079 [Phys. Rev. D (to be published)].
- [10] BES Collaboration, J. Z. Bai *et al.*, Nucl. Instrum. Methods Phys. Res., Sect. A **458**, 627 (2001).
- [11] BES Collaboration, J. Z. Bai *et al.*, Phys. Rev. D **60**, 072001 (1999).
- [12] D. Aston *et al.*, Nucl. Phys. **B296**, 493 (1988).
- [13] Mark I Collaboration, W. Tanenbaum *et al.*, Phys. Rev. D **17**, 1731 (1978); G. Karl, S. Meshkov, and J. L. Rosner, *ibid.* **13**, 1203 (1976); Crystal Ball Collaboration, M. Oreglia *et al.*, *ibid.* **25**, 2259 (1982).
- [14] X. H. Mo *et al.*, High Energy Phys. Nucl. Phys. **28**, 455 (2004).
- [15] BES Collaboration, J. Z. Bai *et al.*, Phys. Rev. D **69**, 012003 (2004).